

# Catalpol prevents denervated muscular atrophy related to the inhibition of autophagy and reduces BAX/BCL2 ratio via mTOR pathway

This article was published in the following Dove Press journal:  
Drug Design, Development and Therapy

Yuan Wang<sup>1,\*</sup>  
Yali Shao<sup>1</sup>  
Yuqing Gao<sup>1</sup>  
Guoran Wan<sup>2</sup>  
Dong Wan<sup>3,\*</sup>  
Huifeng Zhu<sup>1</sup>  
Yan Qiu<sup>1</sup>  
Xiyue Ye<sup>1</sup>

<sup>1</sup>Department of Chinese Medicine, College of Pharmaceutical Sciences and Traditional Chinese Medicine, Southwest University, Chongqing Engineering Research Center for Pharmacological Evaluation, Chongqing 400715, China;

<sup>2</sup>Department of Clinic Medicine, Chongqing Three Gorges Medical College, Chongqing 404120, China; <sup>3</sup>Department of Emergency, The First Affiliated Hospital of Chongqing Medical University, Chongqing 400016, China

\*These authors contributed equally to this work

**Aim:** To investigate the effects of catalpol on muscular atrophy induced by sciatic nerve crush injury (SNCI).

**Methods:** Seventy male Kunming mice were randomized into five groups (n=10): model, sham, catalpol (Cat), rapamycin (Rapa), and catalpol+rapamycin (Rapa+Cat). The ratio of gastrocnemius muscle wet weight (right/left, R/L) between the operated leg (right) and the normal leg (left) was calculated, and acetylcholinesterase (AChE) immunohistochemistry assays were performed to observe the change of motor end plate (MEP), along with the sizes of denervated and innervated muscle fibers. The expression levels of LC3II, TUNEL, BAX/BCL-2, LC3II/LC3I and P62, Beclin1, mTOR, and p-mTOR (ser2448) proteins in muscle were examined by fluorescence immunohistochemistry or Western blotting.

**Results:** Results show that catalpol improved the results of the grid walking tests by reducing the percentage of foot slips, which increased the gastrocnemius muscle wet weight (R/L), enhanced AChE expression at the MEP, and enlarged the section area of the muscle. The expression of LC3II and TUNEL was significantly inhibited by catalpol. The BAX/BCL-2 ratio was significantly increased in muscles of denervated and control groups. Lower LC3II/LC3I and BAX/BCL-2 ratios in denervated muscles were also detected after catalpol treatment.

**Conclusion:** These results indicated that apoptosis and autophagy play a role in the regulation of denervation-induced muscle atrophy after SNCI, and catalpol alleviates muscle atrophy through the regulation of muscle apoptosis and autophagy via the mTOR signaling pathway.

**Keywords:** catalpol, sciatic nerve crush injury, SNCI, denervated muscle atrophy, autophagy, muscle apoptosis

## Introduction

PNI is a complex injury which is usually caused by stab wounds, direct trauma, sharp injury, crush, fall, war, fracture, gunshot wound, obstetric trauma, laceration, and dislocation.<sup>1</sup> They have a high incidence (1.3%–2.8%) among adult males and people of a productive age, and can significantly affect their quality of life, while most of them require high-cost surgery and treatment.<sup>2,3</sup>

PNI is the most common causes of muscular atrophy in adults,<sup>4</sup> leading to Wallerian degeneration and disruption of axonal connections at the lesion site.<sup>5</sup> When motor neurons fail to conduct impulses from the CNS to skeletal muscles, mass and contractile force of denervated muscle would be reduced, as well as the morphology, ultrastructure, gene expression pattern, and biochemistry of myofibers and the surrounding tissues can be altered.<sup>6</sup> Nerve injuries trigger complex cellular

Correspondence: Huifeng Zhu  
Department of Chinese Medicine,  
College of Pharmaceutical Sciences,  
Southwest University, 2 Tiansheng Road,  
Beibei District, Chongqing 400716, China  
Tel +86 23 6825 1225  
Email zhfbsci@126.com;  
zhfbwu@swu.com.cn

and molecular interactions that are essential for axonal regeneration and functional recovery of patients.<sup>7</sup> Although autophagy is an important pro-survival mechanism to eliminate toxic proteins and damaged organelles in the cells,<sup>8</sup> it may play a different role in PNIs.<sup>4,8,9</sup> Thus, the exact role of autophagy in muscular atrophy induced by PNIs and how it can be modulated by PNIs remain unclear, which may indicate some new targets for an effective pharmacological correction to promote nerve regeneration and reestablish motor function.<sup>6,9</sup>

*Rehmannia glutinosa* Libosch, a traditional Chinese herb which is widely used in clinical treatment, has the functions of storing energy, replenishing substance required by human body and improving the development, which has great medicinal value. Studies have reported that *Rehmannia glutinosa* and its active principles have effects on pharmacological functions of the blood system, immune system, endocrine system, cardiovascular system, nervous system, etc.<sup>10</sup> Catalpol, an iridoid glucoside from *Rehmannia glutinosa* Steud,<sup>10</sup> protects brain neurons in ischemia,<sup>11,12</sup> alleviates neuropathic pain,<sup>13</sup> and ameliorates diabetic encephalopathy in rats.<sup>14</sup> Our own studies and data from other groups suggest that catalpol can exert some positive effects, such as promoting brain angiogenesis in stroke<sup>15</sup> and improving memory in a rat dementia model.<sup>16–21</sup> However, the effects of catalpol on PNIs and the mechanism of skeletal muscle atrophy induced by PNIs remain unclear. Here, we analyzed the ability of catalpol to prevent skeletal muscles from atrophy induced by sciatic nerve crush injury (SNCI). We also examined whether the effects of alleviating denervated muscle atrophy have a relationship with the inhibition of autophagy and apoptosis.

## Materials and methods

### Reagent and drugs

Catalpol was purchased from Liubobainiao Biotechnology Co., Ltd (Shijiazhuang, China), with the purity of 99%, as assayed by the high-performance liquid chromatography analysis. Rapamycin was purchased from Bioduly Biotechnology Co., Ltd. (Nanjing, China). Acetylcholinesterase was obtained from Sigma-Aldrich (St Louis, MO). The TUNEL BrightRed Apoptosis Detection Kit was purchased from Vazyme Biotechnology Co., Ltd. (Nanjing, China).

### Animals and group

In total, 70 adult male Kunming mice (weighing 25–30 g, age 5 weeks) were purchased from the Animal Center, Chongqing Medical University (Chongqing, China). All the

mice were randomly divided into five groups (n=10 per group): model group, sham group, catalpol group (Cat), rapamycin group (Rapa), and rapamycin+catalpol group (Rapa+Cat). All the mice had free access to water and food and were maintained at constant temperature (25°C±1°C) and humidity (55%±5%) under a 12-hour light/dark cycle (07:00 hours light on, 19:00 hours light off).

### Ethics statement

All the procedures strictly complied with the 3R principles, whereas animal care and housing procedures were in full compliance with the national regulatory guidelines. The protocol of this study was approved prior to implementation by the Ethics Committee of Southwest University, and all procedures were in accordance with the National Institutes of Health Guide for the Care and Use of Laboratory Animals. Special care was taken to minimize the number of animals used and animal suffering.

### Surgical procedures and drug administration

Except for the sham group, each animal underwent an aseptic operation with 3.5% chloral hydrate (Production code: 201200321, Sino Pharm Chemical Reagent Co., Ltd, Beijing, China) anesthesia by a qualified technician to expose the right sciatic nerve. The nerve was then crushed at 5 mm proximal to the trifurcation of the sciatic nerve with sterile forceps (width: 2.0 mm) and rotated 90° for 60 seconds. The body temperature of mice was maintained at 37°C with a homothermal blanket. Catalpol dosages were selected based on previous studies<sup>18</sup> and preliminary experiments. Catalpol (10 mg/kg) was dissolved in physiological saline, and administered once a day by intraperitoneal injection for 7 days. Rapamycin (5 mg/kg) was dissolved in 200 µL DMEM (from a 10 mg/mL stock solution) in DMSO, and was intraperitoneally injected for 2 days after the clamp injury. In the Rapa+Cat group, rapamycin was intraperitoneally injected 1 hour before sciatic nerve clamp injury, and catalpol (10 mg/kg) was administered 2 hours after operation. Mice in the sham group and the model group received physiological saline at the dose of 1 mL/kg.

### Functional assessment: grid walking test

The grid walking test was used to assess the ability of mice to accurately place the forepaws during spontaneous exploration, as described previously<sup>22,23</sup> with minor modifications, by analyzing the frequency of failed grasping of the rungs. Briefly, mice were placed on a device with rectangular grid

wire used to observe and evaluate the behavior of the mice (400×300 mm in oblong shape with 80×10 mm grid squares) and allowed to freely explore the area for 3 minutes. The mice were videotaped and later examined off-line by an experimenter blinded to the treatment groups, who scored the percentage of foot slips per the first 100 steps. A foot slip was scored either when the paw completely missed the rung, or when the paw was correctly placed on the rung but slipped off during weight bearing. All the animals received no special pretraining in this task but were placed on the grid twice before the treatment for habituation to handling and to obtain baseline scores.

### Gastrocnemius muscle wet weight

The gastrocnemius muscles from both (the operated and contralateral nonoperated) limbs were dissected, removed, put/placed on an absorbent filter paper, and then weighed using an analytical balance. Both the left (nonoperated side) and right (operated side) gastrocnemius muscles were carefully cleaned and resected, and the gastrocnemius muscle weight ratio (right/left, R/L) was calculated, as described previously.<sup>24</sup>

### Muscle tissue repair

Seven days after the surgery, six mice in each group were deeply anesthetized with an overdose of 3.5% chloral hydrate (0.1 mL/10 g, i.p), and transcardially perfused with 0.9% NaCl solution to rinse out the blood, followed by perfusion with 250 mL of 4% formalin (4°C) to fix the muscle tissue. The muscle tissue was postfixed in 4% paraformaldehyde and subsequently cut into 6 µm coronal sections by a cryostat (Leica CM1900, Germany) for HE staining, acetylcholinesterase assay, and TUNEL and LC3-II staining by fluorescent immunohistochemical technology. Another eight muscle tissue samples in each group were immediately frozen using liquid nitrogen and stored at -70°C until further analysis. Serial transverse 6-µm-thick sections were cut by a cryostat (Leica CM1900). Ipsilateral muscles (0.1 g per muscle) in each group were also weighed for Western blotting analysis of LC3II/LC3I, BCL2/BAX, and mTOR signaling protein, and biochemical determination of SOD and MDA.

### Muscle collection from operated limbs and biochemical determination

Muscle samples were collected from mice after sacrifice with overdose anaesthetic after 7-day-long catalpol treatment, and centrifuged at 5,120×g for 20 minutes at 4°C for 1 hour after

collection for obtaining supernatant. Then the activities of SOD and the concentration of MDA were measured with commercially available kits.

### Gastrocnemius muscle section area

For morphometric analysis of gastrocnemius muscle, fixed tissue specimens were washed in physiological saline and embedded in Tissue-Tek O.C.T. compound to be positioned more easily in the microtome and have better qualities during sectioning. Serial 6-µm-thick sections were obtained by Frozen Slicer (Leica CM1900) and mounted onto polylysine-coated slides according to the reference.<sup>25</sup> HE staining was performed on every sixth section of each specimen and visualized by light microscopy (OPTEC, BK6000, Chongqing, China). Images from six random visual fields were acquired for the sixth stained sections of each specimen using an OPTEC BK6000 microscope (20× objective at 2,048×2,048 resolution with 1.6-times zoom) and then digitized through the affiliated Image-Pro-Plus 6.0 (IPP) software (Media Cybernetics, Rockville, MD, USA). The CSA of muscle fibers was quantitatively analyzed using IPP. The morphometric analysis was performed by two independent investigators blinded to the treatments.

### Acetylcholinesterase assay

Acetylcholinesterase (AChE) assay was used to determine the distribution of AChE on the MEP of the gastrocnemius muscle. In addition, the intensity of the staining was recorded to assess the activity of this enzyme. The muscles were embedded in Tissue-Tek O.C.T. compound and serial 6-µm-thick sections were cut by Frozen Slicer and mounted onto polylysine-coated slides. Staining was performed according to standard protocols.<sup>39,40</sup>

### In situ tailing of nuclear DNA fragmentation (TUNEL)

The TUNEL technique was used to detect DNA fragmentation in situ with a commercial Bright Red Apoptosis Detection Kit (Vazyme, Nanjing, China). Briefly, serial 10 µm sections of muscle sample (Leica CM1900) were fixed with 4% paraformaldehyde in PBS for 1 hour, and permeabilized with 0.1% Triton X-100 and 0.1% sodium citrate in PBS for 2 minutes. TUNEL reaction was performed. After TUNEL labeling, nucleus was labeled with DAPI in blue and the TUNEL-positive-labeled cells were in red, which were observed by Olympus IX71 fluorescence microscope (Olympus, Japan; 20× objective at 1,024×1,024 resolution

with 1.6-times zoom). The morphometric analysis was performed by two independent investigators blinded to the treatments.

## Muscles LC3II stained with fluorescence immunohistochemical technology

The basal level of LC3 (microtubule-associated protein 1 light chain 3) isoforms, key markers of autophagy, was measured in mice muscles to compare the degree of autophagy induction (ie, autophagic flux) in each group by using fluorescence immunohistochemical technology. Animal muscle tissues were transcardially perfused and fixed with 4% paraformaldehyde, cryopreserved in 30% sucrose, and cut into three series of consecutive sections (10  $\mu$ m) in cryostat. Each set of tissue sections was immunostained with the rabbit polyclonal antibody-against LC3II (1:200, CST, Danvers, MA, USA), and then incubated with FITC-labeled goat anti-mouse IgG (Proteintech, Wuhan, China). The nucleus was stained with DAPI in blue. After washing, immunostained cells were observed under a Nikon microscope and were documented with a Nikon digital camera (Japan).

## Western blot analysis

After rinsing with 0.9% NaCl, gastrocnemius muscles (0.1 g per muscle) in each group were separated and weighed for detecting the expression of LC3I, LC3II, P62, Beclin1, BCL2, BAX, mTOR, and p-mTOR by Western blotting. Gastrocnemius muscles were lysed on ice in a lysis buffer [50 mM Tris-HCl (pH 8.2), 0.5 M saccharose, 10 mM HEPES (pH 7.9), 1.5 mM MgCl<sub>2</sub>, 10 mM KCl, 1 mM EDTA, 10% (v/v) glycerine, 1 mM DTT, 1 mM PMSF, 10  $\mu$ g/mL aprotinin, and 5  $\mu$ g/mL leupeptin], as described earlier.<sup>15</sup> After centrifugation at 12,000 rpm for 5 minutes, protein content in cleared lysate was determined by Bradford Assay. Lysate samples containing 40  $\mu$ g lysate protein were fractionated by 5% SDS-PAGE gels and then transferred onto polyvinylidene fluoride (PVDF) membranes (Millipore Sigma, IPVH00010, Burlington, MA, USA). The membranes were probed with primary rabbit polyclonal antibodies, including BCL2 (1:300), BAX (1:2,000, Proteintech, Wuhan, China), LC3I (1:1,000), LC3II (1:1,000), P62 (1:1,000), Beclin1 (1:1,000), p-mTOR (ser2448) (1:1,000, CST, Boston, MA), mTOR (1:500), GAPDH (1:5,000), or beta-tubulin (1:1,000, Proteintech), which was used as a loading control, in 5% bovine serum albumin in Tris-buffered saline (TBS). Twenty-four hours after TBST [TBS with Tween 20 (0.1%)] rinsing, HRP secondary antibodies and anti-rabbit IgG HRP (Proteintech) were incubated

with the immunoblot at a 1:5,000 dilution for 1 hour at room temperature. The PVDF membrane was then put into ECL solution. The result of protein detection was digitally scanned by Tanon 5,200 (Tanon, Shanghai, China) system and quantified using ImageJ (National Institutes of Health, Bethesda, MD, USA) software. GAPDH and beta-tubulin were used as internal controls for all Western blotting assays.

## Statistical analysis

Myocytes collected from five areas were randomly selected from each section, and an area including 100 muscle fibers was counted by an observer blinded to the slides. DAPI-positive nuclei (blue), TUNEL-positive (red), or LC3II-positive (green) nuclei were identified and counted. The apoptosis or autophagy ratio in gastrocnemius muscle was calculated by the ratio of TUNEL or LC3II-positive cell to total nuclei of muscle fibers in the defined area. The number of TUNEL-stained cells, LC3II-stained cells, and the intensity of staining were analyzed by IPP Version 6.0 software. Five fields of each slice were randomly selected for blinded scoring and analysis. All experiments were performed in triplicate. The SPSS 19.0 software was employed for statistical analysis using one-way analysis of variance (ANOVA, factor: group) along with the post-hoc Tukey's test. *P*-values <0.05 were deemed statistically significant.

## Results

### General observations after surgery

During surgery, the animals were monitored for 1–3 hours post-anesthesia, with the 100% perioperative survival rate. All animals in the control and experimental groups survived the surgery period and exhibited normal eating and drinking behavior. The model animal showed no signs of infection and postoperative symptoms (except for sham operation), such as limp toed gait and claw foot swelling after surgery.

### Catalpol improved functional outcome after sciatic nerve crush injury and reversed the inhibitory effect of Rapa in the grid walking test

Baseline scores in each group before SNCI showed no difference in mouse walking. At the end of days 1, 4, and 7, the sham group mice showed an increased slip errors rate, which was significantly lower than that in the model group, confirming the success of modeling. The grid walking test results showed that the percentage of foot slip errors increased after SNCI; however, catalpol reduced this

**Table 1** The percentage of foot slips in the experimental groups in the grid walking test (mean±SD, n=10)

Group	n	Dose (0.1 mL/10 g)	Before nerve injury	After nerve injury with treatment		
				1 day	4 days	7 days
Model	8	0.2	0	73.71±5.2*	70.32±4.34*	65.08±3.55*
Sham	8	0.2	0	9.64±1.9	10.24±1.88	10.87±1.63
Cat	8	0.2	0	60.04±3.54 <sup>#</sup>	48.66±2.65 <sup>###</sup>	30.48±3.22 <sup>###</sup>
Rapa+Cat	8	0.2	0	55.36±4.02 <sup>*</sup>	42.24±3.93 <sup>**</sup>	37.61±3.04 <sup>**</sup>
Rapa	8	0.2	0	70.43±4.90	69.63±4.09	62.37±3.45

**Notes:** \* $P<0.05$  vs sham-operated group; <sup>#</sup> $P<0.05$ , <sup>###</sup> $P<0.01$  vs model group; <sup>\*</sup> $P<0.05$ , <sup>\*\*</sup> $P<0.01$  vs rapamycin group.

**Abbreviations:** Cat, catalpol; Rapa, rapamycin.

percentage significantly following 1 day ( $P<0.05$ ), 4 days, and 7 days ( $P<0.01$ ) of treatment. No significant difference was observed in the Rapa vs the model group ( $P>0.05$ ). Compared with the Rapa group, catalpol reduced the effects of Rapa following 1 day ( $P<0.05$ ), 4 days, and 7 days ( $P<0.01$ ) of treatment (Table 1).

## Catalpol prevented target gastrocnemius muscle atrophy following sciatic nerve injury

As shown in Figure 1A, morphological atrophy of target gastrocnemius muscles was observed 7 days after sciatic nerve injury. The sciatic nerve injury caused a reduction in neural innervation of the gastrocnemius muscle, leading to reduced muscle weight. The sham group and catalpol group maintained polygonal muscle fibers with polynuclei. Catalpol treatment improved the gastrocnemius muscle structure, leading to an increase in muscle weight.

Figure 1B illustrates sections of gastrocnemius muscles stained with HE. The model and Rapa groups exhibited pathological changes, with decreased muscle wet weight ratio

and unclear irregular ultrastructure of myofibrils. Myofibril atrophy spreading, cell denaturation, cell membrane damage, and partial necrosis of muscle cells were observed in these two groups by optical microscopy.

As shown in Table 2, the reduction was quantified by weighing the muscles from operated and normal leg and calculating the muscle weight ratio (R/L) by dividing the weight of the experimental muscle (right) with that of the control muscle (left). In addition, muscle fiber atrophy degree was determined by the wet weight ratio and the CSA of muscle fibers. After injury, both the muscle wet weight ratio and the CSA of muscle fibers decreased compared with those of the sham group ( $P<0.01$ ), while the catalpol treatment significantly increased both the muscle wet weight ratio and the CSA of muscle fibers ( $P<0.05$ ). Rapa treatment decreased both the wet weight ratio and the CSA of muscle fibers ( $P<0.01$ ), whereas catalpol+Rapa treatment reversed the inhibitory effect of Rapa on muscle fibers ( $P<0.01$  vs Rapa). These results suggested that catalpol may promote recovery of the innervation of the gastrocnemius muscle, and counteract the effects of the mTOR signaling inhibitor Rapa.

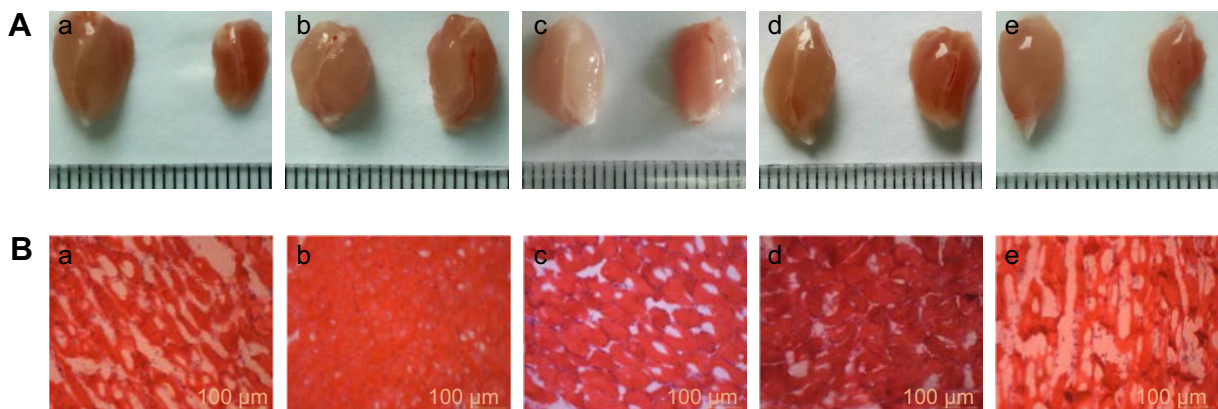


**Figure 1** Catalpol reduced muscle atrophy at day 7 as determined by HE staining (200×).

**Notes:** (A) Photographs of muscle atrophy at day 7 after treatment (experimental muscles are on the right, and contralateral muscles are on the left); (B) Light micrographs of transverse-sectioned gastrocnemius muscle with HE staining. (a) Model group. (b) Sham-operated group. (c) Catalpol group. (d) Rapamycin+catalpol group. (e) Rapamycin group. Scale bar = 100 μm.

**Abbreviation:** HE, Hematoxylin and Eosin.

**Table 2** Effect of catalpol on gastrocnemius muscle wet weight ratio and gastrocnemius muscle section area (mean±SD, n=6)

Group	Muscle wet weight ratio (%)	Muscle section area (μm)
Model	63.01±2.37*	601.21±58.94*
Sham	98.78±1.08	1,065.83±97.08
Cat	78.25±2.69#	876.67±98.49#
Rapa+Cat	72.74±5.10**	792.80±67.75**
Rapa	59.61±3.32	613.35±51.32

**Notes:** \* $P<0.05$  vs sham operated group; # $P<0.05$  vs model group; \*\* $P<0.01$  vs rapamycin group.

**Abbreviations:** Cat, catalpol; Rapa, rapamycin.

## Catalpol inhibited MEP number and size change due to the sciatic nerve injury detected by acetylcholinesterase enzyme histochemistry

AChE immunostaining was applied to characterize MEP morphology in all five groups. The MEP bands corresponded to the terminal nerve branches. The MEP of the sham group was smooth, with a clear structure and deep staining (Figure 2A). With regard to the staining of the model group, MEP was lightly stained, and blur margins appeared along with irregular shapes (Figure 2B). The MEP staining of the rapamycin group was light, which indicated signs of degeneration and disintegration (Figure 2E). In contrast, catalpol treatment leads to better results of AChE assays, in terms of the increased number of MEP, along with the shape of MEP being more intact and similar to that of the sham group (Figure 2C). In the Rapa+Cat group, the number of MEP increased significantly compared with the model and rapamycin groups (Figure 2D). These findings suggested that catalpol may increase the expression of the acetylcholinase and the mature AChE receptor on the MEP, indicating the restoration of peripheral nerve after the injuries. Taken together, these findings indicate that catalpol treatment can significantly increase MEPs and protect skeletal muscles from denervation via activating the mTOR pathway.

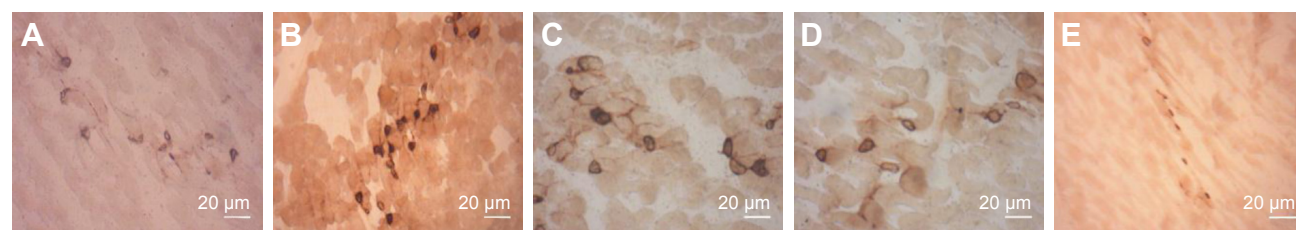


**Figure 2** Catalpol improved the state of MEP as determined by AChE staining (200×).

**Notes:** (A) Model group. (B) Sham-operated group. (C) Catalpol group. (D) Rapamycin+catalpol group. (E) Rapamycin group. Scale bar =20 μm.

**Abbreviations:** AChE, acetylcholinesterase; MEP, motor end plate.

## Effect of catalpol on SOD activity and MDA content of gastrocnemius muscle

The activity of antioxidative enzymes SOD and the concentration of MDA in plasma are shown in Table 3. Overall, there were significant differences in oxidative stress between the model and the sham groups ( $P<0.05$ ), whereas the nerve injury decreased SOD activity and increased MDA content in the target gastrocnemius muscle. Catalpol significantly improved the activity of SOD and decreased MDA concentration ( $P<0.05$  vs model), and reversed the effects of Rapa (inhibitor of mTOR signal), which decreased SOD activity and increased MDA concentration in denervated atrophy muscle ( $P<0.05$  vs Rapa).

## Catalpol inhibited autophagy (LC3II, green) and apoptosis (TUNEL, red) of denervated gastrocnemius muscle

As shown in Figure 3, compared with the sham group, the number of LC3II (green) muscle cells as well as TUNEL (red) muscle cells increased significantly ( $P<0.05$  vs sham). Catalpol significantly reduced the number of LC3II and TUNEL cells compared with those in the model group ( $P<0.05$  vs model). Rapa, the autophagy activator, increased the number of LC3II cells and the apoptosis ratio of the muscle cells, whereas catalpol reversed these inhibitory effects of Rapa ( $P<0.05$  vs Rapa).

## The effects of catalpol related to mTOR signaling

### Catalpol inhibited autophagy moderately in denervated muscle via mTOR signaling

Compared with the normal group, the LC3II expression level in the model muscle significantly increased ( $P<0.05$ ), while catalpol at 10 mg/kg reduced autophagy marker LC3II expression and the ratio of LC3II/LC3I ( $P<0.05$ ) compared

**Table 3** Effect of catalpol on SOD activity and MDA content in the gastrocnemius muscle (mean $\pm$ SD, n=6)

Group	SOD activity U/mg	MDA Nmol/mg
Model	4.98 $\pm$ 0.06*	1.58 $\pm$ 0.07*
Sham	6.23 $\pm$ 0.05	1.32 $\pm$ 0.06
Cat	5.49 $\pm$ 0.06#	1.51 $\pm$ 0.09#
Rapa+Cat	5.02 $\pm$ 0.09&	1.42 $\pm$ 0.06&
Rapa	3.61 $\pm$ 0.32	1.85 $\pm$ 0.12

**Notes:** \* $P$ <0.05 vs sham-operated group; # $P$ <0.05 vs model group; & $P$ <0.05 vs rapamycin group.

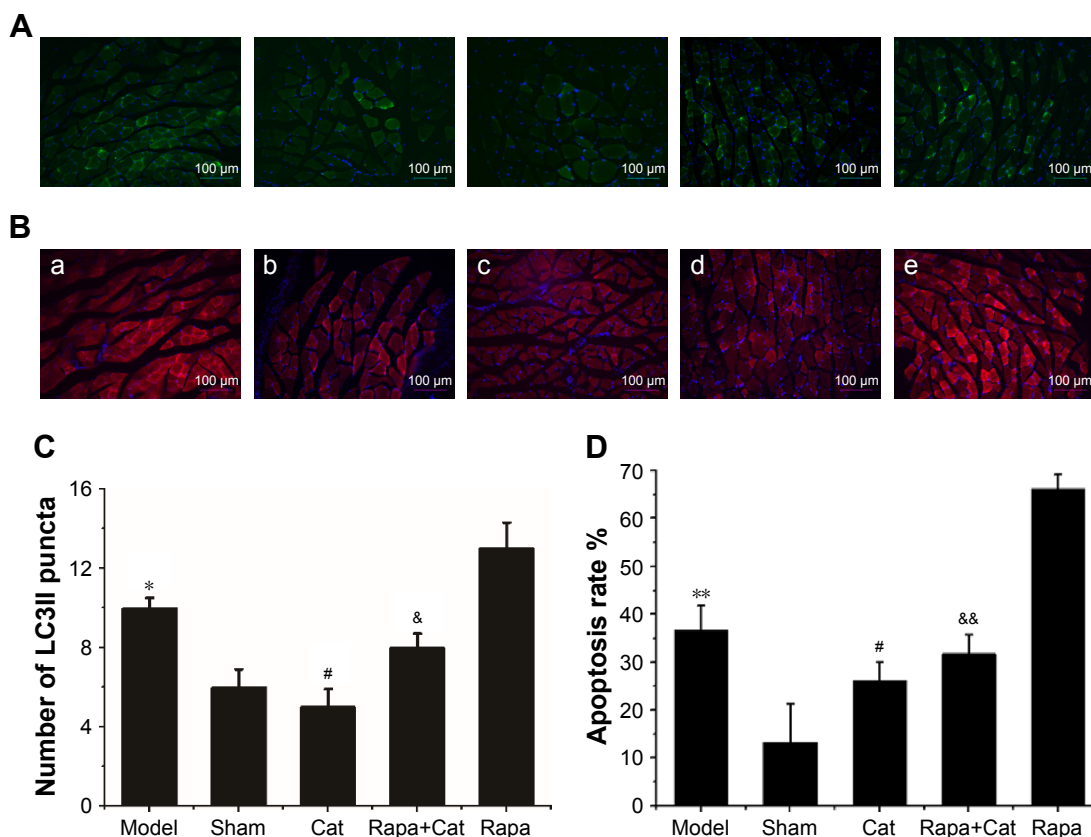
**Abbreviations:** Cat, catalpol; Rapa, rapamycin; SOD, superoxide dismutase; MDA, malondialdehyde.

to that of the model group. Rapa, an mTOR signal inhibitor and autophagy activator, significantly inhibited mTOR phosphorylation, reduced the ratio of p-mTOR/mTOR, activated LC3II expression, and increased the ratio of LC3II/LC3I. Catalpol also reversed the inhibitory effect of Rapa on mTOR signaling, LC3II expression, and LC3II/LC3I ratio, which indicated that the effects of catalpol on denervated muscle autophagy were related to mTOR signaling. p62 and Beclin1

proteins, which are also closely related to autophagy and apoptosis,<sup>26-29</sup> were accumulated in the denervated muscle after SNCI ( $P$ <0.05). After catalpol treatment, Beclin1 expression was decreased and P62 protein expression showed an increment ( $P$ <0.01). Catalpol also reversed the inhibitory effect of Rapa on p62 and Beclin1 protein expression ( $P$ <0.05, Figure 4).

### Catalpol protected denervated muscle against pro-apoptotic processes via mTOR signaling

To further determine the effects of catalpol on apoptosis of denervated muscle cells, the protein levels of BCL-2 in the denervated muscle cells of gastrocnemius muscle were determined. Quantitative analysis by Western blotting showed that catalpol treatment decreased the level of BAX as compared to that in the model (58.13%) and rapamycin (63.4%) groups. Catalpol treatment significantly inhibited BAX activation and reduced the level of BAX. Furthermore, catalpol treatment

**Figure 3** Suppression of autophagy and apoptosis by catalpol during the acute phase of sciatic nerve crush injury.

**Notes:** (A) Representative immunofluorescent images of staining with LC3II (green) and DAPI (blue) in mice denervated atrophy muscle 7 days after SNCI; (B) Representative immunofluorescent images of staining with TUNEL (red) and DAPI (blue) in mice denervated atrophy muscle 7 days after SNCI [a] Model group. [b] Sham-operated group. [c] Catalpol group. [d] Rapamycin+catalpol group. [e] Rapamycin group; (C) Quantitative analysis of the number of LC3-positive and (D) TUNEL-positive cells. \* $P$ <0.05 vs sham-operated group; # $P$ <0.05 vs model group; & $P$ <0.05, && $P$ <0.01 vs rapamycin group. Scale bar = 100  $\mu$ m.

**Abbreviations:** Cat, catalpol; Rapa, rapamycin; SNCI, sciatic nerve crush injury; TUNEL, terminal deoxynucleotidyl transferase (TdT)-mediated dUTP nick end labeling.

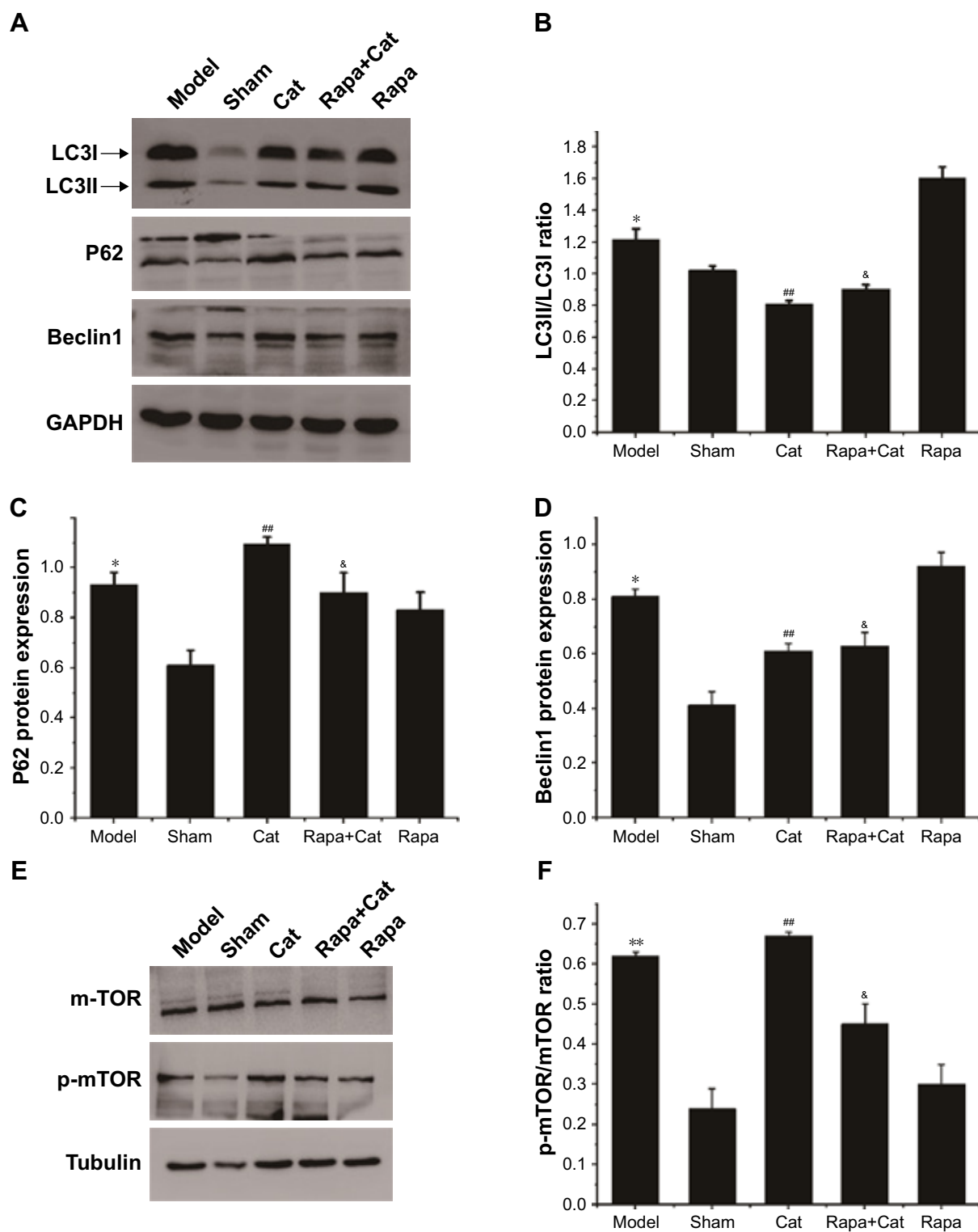


**Figure 4** Effects of catalpol on LC3II/LC3I, P62, Beclin1, and p-mTOR/mTOR level in each group as determined by Western blot analysis.

**Notes:** (A) Expression of LC3II/LC3I, P62, and Beclin1 analyzed by Western blotting; (B–D) Quantification of expression of LC3II/LC3I, P62, and Beclin1 by Western blots, respectively; (E) Expression of p-mTOR/mTOR analyzed by Western blots; (F) Quantification of the p-mTOR/mTOR ratio in each group by Western blots. \* $P < 0.05$ , \*\* $P < 0.01$  vs sham-operated group; ## $P < 0.01$  vs model group; & $P < 0.05$  vs rapamycin group.

**Abbreviations:** Cat, catalpol; Rapa, rapamycin.

increased the level of BCL-2 as compared to that in the model (40.3%) and rapamycin (48.73%) groups. The results of BAX and BCL-2 supported the antiapoptotic effects of catalpol on the denervated gastrocnemius muscle cells following

sciatic nerve injury (Figure 5). These data indicate that catalpol treatment protects motor neurons by inhibiting the pro-apoptotic pathway in sciatic nerve-injured mice, and that these effects are linked to mTOR signaling.

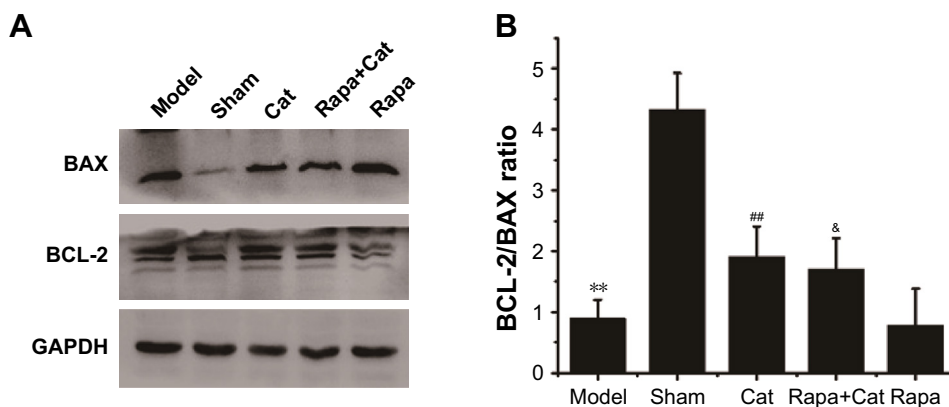


**Figure 5** Catalpol reduced BAX and increased BCL-2 and the ratio of BCL-2/BAX level as determined by Western blots analysis.

**Notes:** (A) Expression of BAX and BCL-2 analyzed by Western blotting; (B) Quantification of BAX/BCL-2 level in each group by Western blots. \*\* $P < 0.01$  vs sham-operated group; ## $P < 0.01$  vs model group; & $P < 0.05$  vs rapamycin group.

**Abbreviations:** Cat, catalpol; Rapa, rapamycin.

## Discussion

In summary, the results presented here show that catalpol accelerated functional recovery after SNCI and reversed the inhibitory effect of Rapa, as assessed by the grid walking test (Table 1). Catalpol prevented denervated muscle atrophy (Figure 1 and Table 2), likely due to inhibition of autophagy in muscle tissue (Figures 3 and 4).

Denervated muscle atrophy as a cause of sarcopenia (the loss of muscle mass and function) is a common symptom of PNIs. Oxidative damage and apoptosis are strongly implicated in this pathogenesis.<sup>30</sup> Functional and morphometric analysis after SNCI demonstrate<sup>6</sup> that muscle atrophy occurs 7 days after the injury, as indicated by decreased muscle wet weight ratio and muscle section area (Table 2), and motor deficits presented by significantly more slips (Table 1), accompanied with oxidative damage and apoptosis (Table 3 and Figures 3 and 5). In contrast, oxidative damage and apoptosis caused by nerve crush injury were alleviated by treatments with catalpol (Table 3 and Figures 3 and 5).

The degradation of cellular constituents may represent a possible mechanism to inhibit cell damage and apoptosis.<sup>30</sup> Since both oxidative damage and apoptosis correlate with autophagy, so inhibiting oxidative products and/or apoptosis to modulate autophagy may be a promising therapeutic strategy to maintain skeletal muscle homeostasis.<sup>31</sup> Autophagy is essential for cellular survival and clearance of damaged proteins and organelles, while excessive autophagy activation can contribute to muscle loss in different catabolic conditions.<sup>32</sup> Autophagy is lower in collagen VI muscular dystrophies, whereas its reactivation promotes myofiber degeneration.<sup>33</sup> Although the role of autophagy in muscle atrophy induced by injured peripheral nerves remains unclear,<sup>6,9,32</sup> our results showed that reduction of muscle area in these model mice was concomitant with increased apoptosis and autophagy, and

that catalpol treatment alleviated the damage caused by nerve crush injury. The regulation of autophagy is fundamental for the skeletal muscle homeostasis in physiological situations and in response to stress. For example, defective or excessive autophagy is harmful for muscle health and has a pathogenic effect on several muscle diseases.<sup>4</sup> In this study, activation of autophagy caused by nerve injury at day 7 and overactivation of autophagy caused by rapamycin accelerated denervated muscle atrophy. Increased ratio of LC3II/LC3I and Beclin1 protein, and deficient P62 expression exacerbated muscle loss and mouse locomotor deficits (Table 1, Figures 2–4), whereas catalpol treatment significantly inhibited muscle loss and markedly improved mouse locomotion (Table 1, Figures 1, 2 and 4). Moreover, catalpol inhibited excessive autophagy caused by rapamycin. We also found that catalpol reversed the elevated LC3II/LC3I and p62 protein level, and decreased Beclin1 expression induced by rapamycin (Figures 3 and 4). These findings provide new mechanistic insights into the role of catalpol in the treatment of muscle loss induced by nerve injury, and its effects on reducing autophagy seem to be associated with mTOR signaling pathway.

In the mouse model, reduction of muscle area was concomitant with increased apoptosis and autophagy (Figures 1 and 3–5). Indeed, autophagy plays a critical role in myofiber maintenance, and its activation is crucial for avoiding the accumulation of toxic proteins and dysfunctional organelles that would lead to muscle atrophy and weakness.<sup>8</sup> Autophagy may, therefore, serve as a mechanism to combat cell damage and apoptosis.<sup>32</sup> Oxidative damage and apoptosis are toxic to the body, and may mediate skeletal muscle degeneration<sup>34,35</sup> and atrophy.<sup>36</sup> Catalpol, known as a free radical scavenging agent,<sup>14,17,37,38</sup> significantly reduces free radical damage in the nerve injury model and prevents muscle apoptosis (Figures 3–5). Increased ratio of BCL-2/BAX and reduced

TUNEL cell count in denervated muscle with inhibition of autophagy relative protein (Figures 3–5) were also observed. Taken together with the rapamycin effects, we conclude that moderating inhibition of autophagy is helpful for denervated muscle recovery, whereas excessive autophagy is detrimental for denervated muscle regeneration. Attenuation of the nerve crush injury-related impairment of autophagy in rodent skeletal muscle may be one of the mechanisms for catalpol to inhibit nerve crush-injury-related cellular damage and cell apoptosis in skeletal muscle *in vivo*.

In line with our findings, the contribution of increased autophagy and apoptosis to muscle atrophy has been shown in a myotonic atrophy type one in *Drosophila*.<sup>8</sup> Other reports show that autophagy inhibition induces atrophy and myopathy in adult skeletal muscles in knockout mice for the critical gene *Atg7* to block autophagy specifically in skeletal muscle,<sup>32</sup> thus necessitating further investigation of the role of autophagy in muscle atrophy after nerve crush injury. While short-term denervation can result in reversible changes in muscle mass, prolonged denervation leads to permanent muscle damage with profound atrophy, myocyte apoptosis, and fibrosis. The type and duration of pathological processes triggered by denervation in muscle atrophy and the effects of catalpol on these processes have not been fully investigated. Our findings suggest that activated autophagy and atrophy of denervated muscle may be mTOR-independent, whereas catalpol intervention at an early stage of muscular pathogenesis can delay damage and/or protect muscle from loss of nerve function and can be related to autophagy inhibition. Together, this implicates catalpol as a promising therapeutic agent to prevent muscle atrophy by modulating autophagy via the mTOR signaling pathway.

## Abbreviations

AchE, acetylcholinesterase; CNS, central nervous system; CSA, cross-sectional area; DMSO, dimethyl sulfoxide; HE, Hematoxylin and Eosin; HRP, horseradish peroxidase-labeled; MDA, Malondialdehyde; MEP, motor end plate; PNIs, Peripheral nerve injuries; PNS, peripheral nervous system; SOD, superoxide dismutase; TBS, Tris-buffered saline; TUNEL, terminal deoxynucleotidyl transferase (TdT)-mediated dUTP nick end labeling.

## Acknowledgment

This work was supported by the National Natural Science Foundation of China (81073084), the Natural Science Foundation Project of CQ (cstc2018jcyjAX0158), Fundamental Research Funds to graduating students for the Central

Universities (XDJK2017D154), and Southwest University Undergraduate Science and Technology Innovation Fund (Project No 20162902001 & YX2017-CXZD-02).

## Author contributions

All authors contributed to data analysis, drafting and revising the article, gave final approval of the version to be published, and agree to be accountable for all aspects of the work.

## Disclosure

The authors report no conflicts of interest in this work.

## References

- Castillo-Galván ML, Martínez-Ruiz FM, de La Garza-Castro O, Elizondo-Omaña RE, Guzmán-López S. Study of peripheral nerve injury in trauma patients. *Gac Med Mex*. 2014;150(6):527–532.
- Lad SP, Nathan JK, Schubert RD, Boakye M. Trends in median, ulnar, radial, and brachiolexus nerve injuries in the United States. *Neurosurgery*. 2010;66(5):953–960.
- Ciaramitaro P, Mondelli M, Logullo F, et al. Traumatic peripheral nerve injuries: epidemiological findings, neuropathic pain and quality of life in 158 patients. *J Peripher Nerv Syst*. 2010;15(2):120–127.
- Grumati P, Bonaldo P. Autophagy in skeletal muscle homeostasis and in muscular dystrophies. *Cells*. 2012;1(3):325–345.
- Sta M, Cappaert NL, Ramekers D, Baas F, Wadman WJ. The functional and morphological characteristics of sciatic nerve degeneration and regeneration after crush injury in rats. *J Neurosci Methods*. 2014;222:189–198.
- Huang HC, Chen L, Zhang HX, et al. Autophagy Promotes Peripheral Nerve Regeneration and Motor Recovery Following Sciatic Nerve Crush Injury in Rats. *J Mol Neurosci*. 2016;58(4):416–423.
- Sulaiman W, Gordon T. Neurobiology of peripheral nerve injury, regeneration, and functional recovery: from bench top research to bedside application. *Ochsner J*. 2013;13(1):100–108.
- Bargiela A, Cerro-Herreros E, Fernandez-Costa JM, Vilchez JJ, Llamusi B, Artero R. Increased autophagy and apoptosis contribute to muscle atrophy in a myotonic dystrophy type 1 *Drosophila* model. *Dis Model Mech*. 2015;8(7):679–690.
- Ning L, Xu Z, Furuya N, Nonaka R, Yamada Y, Arikawa-Hirasawa E. Perlecan inhibits autophagy to maintain muscle homeostasis in mouse soleus muscle. *Matrix Biol*. 2015;48:26–35.
- Zhang RX, Li MX, Jia ZP. *Rehmannia glutinosa*: review of botany, chemistry and pharmacology. *J Ethnopharmacol*. 2008;117(2):199–214.
- Liu YR, Lei RY, Wang CE, et al. Effects of catalpol on ATPase and amino acids in gerbils with cerebral ischemia/reperfusion injury. *Neurol Sci*. 2014;35(8):1229–1233.
- Cai QY, Chen XS, Zhan XL, Yao ZX. Protective effects of catalpol on oligodendrocyte death and myelin breakdown in a rat model of chronic cerebral hypoperfusion. *Neurosci Lett*. 2011;497(1):22–26.
- Wang Y, Zhang R, Xie J, Lu J, Yue Z. Analgesic activity of catalpol in rodent models of neuropathic pain, and its spinal mechanism. *Cell Biochem Biophys*. 2014;70(3):1565–1571.
- Wang CF, Li DQ, Xue HY, Hu B. Oral supplementation of catalpol ameliorates diabetic encephalopathy in rats. *Brain Res*. 2010;1307:158–165.
- Zhu HF, Wan D, Luo Y, Zhou JL, Chen L, Xu XY. Catalpol increases brain angiogenesis and up-regulates VEGF and EPO in the rat after permanent middle cerebral artery occlusion. *Int J Biol Sci*. 2010;6(5):443–453.
- Ahn SM, Kim YR, Kim HN, et al. Neuroprotection and spatial memory enhancement of four herbal mixture extract in HT22 hippocampal cells and a mouse model of focal cerebral ischemia. *BMC Complement Altern Med*. 2015;15:202.

17. Zhou H, Liu J, Ren L, et al. Relationship between [corrected] spatial memory in diabetic rats and protein kinase C $\gamma$ , caveolin-1 in the hippocampus and neuroprotective effect of catalpol. *Chin Med J*. 2014; 127(5):916–923.
18. Wan D, Xue L, Zhu H, Luo Y. Catalpol Induces Neuroprotection and Prevents Memory Dysfunction through the Cholinergic System and BDNF. *Evid Based Complement Alternat Med*. 2013;2013:1–9.
19. Xia Z, Zhang R, Wu P, Xia Z, Hu Y. Memory defect induced by  $\beta$ -amyloid plus glutamate receptor agonist is alleviated by catalpol and donepezil through different mechanisms. *Brain Res*. 2012;1441:27–37.
20. Zhang A, Hao S, Bi J, et al. Effects of catalpol on mitochondrial function and working memory in mice after lipopolysaccharide-induced acute systemic inflammation. *Exp Toxicol Pathol*. 2009;61(5):461–469.
21. Zhang XL, An LJ, Bao YM, Wang JY, Jiang B. d-galactose administration induces memory loss and energy metabolism disturbance in mice: protective effects of catalpol. *Food Chem Toxicol*. 2008;46(8): 2888–2894.
22. Abo-Grisha N, Essawy S, Abo-Elmatty DM, Abdel-Hady Z. Effects of intravenous human umbilical cord blood CD34+ stem cell therapy versus levodopa in experimentally induced Parkinsonism in mice. *Arch Med Sci*. 2013;9(6):1138–1151.
23. Menet V, Prieto M, Privat A, Giménez Y, Ribotta M. Axonal plasticity and functional recovery after spinal cord injury in mice deficient in both glial fibrillary acidic protein and vimentin genes. *Proc Natl Acad Sci U S A*. 2003;100(15):8999–9004.
24. Gu J, Liu H, Zhang N, et al. Effect of transgenic human insulin-like growth factor-1 on spinal motor neurons following peripheral nerve injury. *Exp Ther Med*. 2015;10(1):19–24.
25. Wu R, Yan Y, Yao J, Liu Y, Zhao J, Liu M. Calpain 3 Expression Pattern during Gastrocnemius Muscle Atrophy and Regeneration Following Sciatic Nerve Injury in Rats. *Int J Mol Sci*. 2015;16(11): 26927–26935.
26. Tanabe F, Yone K, Kawabata N, et al. Accumulation of p62 in degenerated spinal cord under chronic mechanical compression: functional analysis of p62 and autophagy in hypoxic neuronal cells. *Autophagy*. 2011;7(12):1462–1471.
27. Gurkar AU, Chu K, Raj L, et al. Identification of ROCK1 kinase as a critical regulator of Beclin1-mediated autophagy during metabolic stress. *Nat Commun*. 2013;4:2189.
28. He C, Zhu H, Li H, Zou MH, Xie Z. Dissociation of Bcl-2-Beclin1 complex by activated AMPK enhances cardiac autophagy and protects against cardiomyocyte apoptosis in diabetes. *Diabetes*. 2013;62(4): 1270–1281.
29. Maejima Y, Kyo S, Zhai P, et al. Mst1 inhibits autophagy by promoting the interaction between Beclin1 and Bcl-2. *Nat Med*. 2013; 19(11):1478–1488.
30. Wohlgemuth SE, Seo AY, Marzetti E, Lees HA, Leeuwenburgh C. Skeletal muscle autophagy and apoptosis during aging: effects of calorie restriction and life-long exercise. *Exp Gerontol*. 2010;45(2):138–148.
31. de Palma C, Perrotta C, Pellegrino P, Clementi E, Cervia D. Skeletal muscle homeostasis in duchenne muscular dystrophy: modulating autophagy as a promising therapeutic strategy. *Front Aging Neurosci*. 2014;6:188.
32. Masiero E, Sandri M. Autophagy inhibition induces atrophy and myopathy in adult skeletal muscles. *Autophagy*. 2010;6(2):307–309.
33. Grumati P, Coletto L, Sabatelli P, et al. Autophagy is defective in collagen VI muscular dystrophies, and its reactivation rescues myofiber degeneration. *Nat Med*. 2010;16(11):1313–1320.
34. Choi MH, Ow JR, Yang ND, Taneja R. Oxidative Stress-Mediated Skeletal Muscle Degeneration: Molecules, Mechanisms, and Therapies. *Oxid Med Cell Longev*. 2016;2016:1–13.
35. Salucci S, Burattini S, Baldassarri V, et al. The peculiar apoptotic behavior of skeletal muscle cells. *Histol Histopathol*. 2013;28(8):1073–1087.
36. Bonaldo P, Sandri M. Cellular and molecular mechanisms of muscle atrophy. *Dis Model Mech*. 2013;6(1):25–39.
37. Zhu H, Wang Y, Liu Z, et al. Antidiabetic and antioxidant effects of catalpol extracted from *Rehmannia glutinosa* (Di Huang) on rat diabetes induced by streptozotocin and high-fat, high-sugar feed. *Chin Med*. 2016;11:25.
38. Li DQ, Bao YM, Li Y, Wang CF, Liu Y, An LJ. Catalpol modulates the expressions of Bcl-2 and Bax and attenuates apoptosis in gerbils after ischemic injury. *Brain Res*. 2006;1115(1):179–185.
39. Baljet B, Drukker J. An acetylcholinesterase method for in toto staining of peripheral nerves. *Stain Technol*. 1975;50(1):31–36.
40. Bellinger DL, Lorton D, Hamill RW, Felten SY, Felten DL. Acetylcholinesterase staining and choline acetyltransferase activity in the young adult rat spleen: lack of evidence for cholinergic innervation. *Brain Behav Immun*. 1993;7(3):191–204.

## Drug Design, Development and Therapy

### Publish your work in this journal

Drug Design, Development and Therapy is an international, peer-reviewed open-access journal that spans the spectrum of drug design and development through to clinical applications. Clinical outcomes, patient safety, and programs for the development and effective, safe, and sustained use of medicines are the features of the journal, which

Submit your manuscript here: <http://www.dovepress.com/drug-design-development-and-therapy-journal>

Dovepress

has also been accepted for indexing on PubMed Central. The manuscript management system is completely online and includes a very quick and fair peer-review system, which is all easy to use. Visit <http://www.dovepress.com/testimonials.php> to read real quotes from published authors.